

Dual-Chirp AFDM for Joint Delay-Doppler Estimation with Rydberg Atomic Quantum Receivers

Hanvit Kim*, Hyeon Seok Rou[†], Kihong Min*, Giuseppe Thadeu Freitas de Abreu[†], and Sunwoo Kim*

*Department of Electronic Engineering, Hanyang University, Republic of Korea

[†]School of Computer Science and Engineering, Constructor University Bremen, Germany

Emails: {dante0813, khmin705, remero}@hanyang.ac.kr, {hrou, gabreu}@constructor.university

Abstract—In this paper, we propose a joint delay-Doppler estimation framework for Rydberg atomic quantum receivers (RAQRs) leveraging affine frequency division multiplexing (AFDM), as a future enabler of hyper integrated sensing and communication (ISAC) in 6G and beyond. The proposed approach preserves the extreme sensitivity of RAQRs, while offering a pioneering solution to the joint estimation of delay-Doppler parameters of mobile targets, which has yet to be addressed in the literature due to the inherent coupling of time-frequency parameters in the optical readout of RAQRs to the best of our knowledge. To overcome this unavoidable ambiguity, we propose a dual-chirp AFDM framework where the utilization of distinct chirp parameters effectively converts the otherwise ambiguous estimation problem into a full-rank system, enabling unique delay-Doppler parameter extraction from RAQRs. Numerical simulations verify that the proposed dual-chirp AFDM shows superior delay-Doppler estimation performance compared to the classical single-chirp AFDM over RAQRs.

Index Terms—Quantum sensing, Rydberg atomic quantum receivers (RAQRs), delay-Doppler estimation, affine frequency division multiplexing (AFDM), ISAC.

I. INTRODUCTION

Next generation integrated sensing and communication (ISAC) for 6G and beyond requires extremely high-quality wireless connectivity and robust sensing capability in the high-mobility scenario [1]. The high-mobility scenario results in a doubly dispersive wireless channel, posing a significant challenge for accurate channel parameter estimations, such as propagation delay and Doppler shifts [2]. To solve this problem, affine frequency division multiplexing (AFDM) waveform has recently been proposed, which enables accurate delay-Doppler estimation by reducing the intercarrier interference (ICI) arising from the severe Doppler shifts in doubly-dispersive channel [3]. Furthermore, its significant implications for standardization highlight its potential as a leading candidate for next-generation wireless systems [4]. Indeed, the AFDM have shown advantages in both sensing and communications functionalities in doubly-dispersive channels compared to the other emerging waveforms for ISAC, such as orthogonal time frequency space (OTFS) [5].

Aside from the waveform design, recent studies are focusing on the Rydberg atomic quantum receivers (RAQRs),

which are envisioned to be a key enabler for high-sensitivity wireless sensing [6]. Harnessing the extreme sensitivity of Rydberg atoms, RAQRs can approach the standard quantum limit (SQL) ($\sim 700\text{pV} \cdot \text{cm}^{-1} \cdot \text{Hz}^{-1/2}$) of electric-field sensitivity, which is significantly lower than the thermal noise of conventional dipole antenna-based receivers [7]. Recently, RAQRs have facilitated significant advancements across various sensing applications, including angle-of-arrival (AOA) estimation [8], Doppler-based localization [9], and ISAC [10].

Despite recent advancements, utilizing RAQRs for precise delay-Doppler estimation remains an unresolved challenge. This is primarily due to two factors: 1) the absence of a system model and framework for joint delay-Doppler estimation with AFDM using RAQRs, and 2) the intrinsic delay-Doppler ambiguity introduced by the optical readout of Rydberg probes in doubly-dispersive channels. While several RAQRs system models have been proposed [11], [12], these consider a single-carrier waveform, which are not applicable for the multi-carrier AFDM-based delay-Doppler estimation. Some initial attempts include range estimation with RAQRs [13], but joint delay-Doppler estimation for 6G ISAC applications still remains an unaddressed issue.

In this article, we address these limitations by proposing a delay-Doppler estimation framework for RAQRs utilizing AFDM waveforms. By deriving the radio frequency (RF)-to-optical measurement model for AFDM signals, we employ the atomic autocorrelation method [13] to map delay-Doppler parameters onto the frequency domain. This analysis reveals that conventional single-chirp AFDM signals yield ambiguous measurements, significantly complicating the joint estimation process. To resolve this, we introduce a dual-chirp AFDM variant that leverages two distinct post-chirp rates, $c_1^{(A)}$ and $c_1^{(B)}$, which facilitates rank-restoration of the estimation model from the optical measurements, enabling unambiguous estimation of the delay and Doppler parameters of the radar targets.

The contributions of the article are summarized as follows:

- The quantum system model for AFDM signal detection is analyzed, and a dedicated framework for joint delay-Doppler estimation utilizing RAQRs is established;
- The dual-chirp AFDM is proposed to resolve the rank-deficient joint delay-Doppler estimation problem, and an least squares (LS)-based estimation algorithm is proposed to achieve high-accuracy parameter recovery.

The fundamental research described in this paper was supported by the National Research Foundation (NRF) of Korea under Grant RS-2024-00409492, and by the German Research Foundation (DFG) through the QUBYSM Project with Grant No. G:(GEPRIS)576171458.

II. SYSTEM MODEL

A. Affine Frequency Division Multiplexing

The transmitted discrete affine Fourier transform (DAFT)-domian vector $x[m]$ is mapped onto the discrete time domain signal $s[n]$ using the inverse DAFT (IDAFT), which is presented as [14]

$$s[n] = \frac{1}{\sqrt{N}} \sum_{m=0}^{N-1} x[m] e^{j2\pi(c_2 m^2 + \frac{1}{N} m n + c_1 n^2)}, \quad (1)$$

where N is the number of chirp subcarriers, and c_1 and c_2 are the pre-chirp and post-chirp parameters of the IDAFT, affecting various properties of AFDM.

Given the above, the continuous time version of the transmitted signal in (1) can be written as [15]

$$s(t) = \sum_{m=0}^{N-1} x[m] e^{j2\pi(c_2 m^2 + \phi_m(t))}, \quad 0 \leq t \leq T. \quad (2)$$

where $T = N\Delta t$, with the Nyquist sampling rate $\frac{1}{\Delta t}$, is the duration of the instantaneous phase function of the m -th chirp $\phi_m(t)$, defined as piece-wise manner as [14]

$$\phi_m(t) = \tilde{c}_1 t^2 + \frac{m}{T} t - \frac{q}{\Delta t} t, \quad t_{m,q} \leq t < t_{m,q+1}, \quad (3)$$

with $\tilde{c}_1 = \frac{c_1}{(\Delta t)^2}$, and $t_{m,q}$ is the q -th spectrum wrapping point of m -th chirp subcarrier. Note that c_1 controls the frequency dispersion of the signal, which can be changed and optimized according to the Doppler characteristics of the doubly dispersive wireless channel [16].

B. Rydberg Atomic Quantum Receiver Model

1) *Quantum state*: The energy level of an atom changes as the photon is either absorbed or emitted. By leveraging this electron transition, the RF signals can be detected. The electron transition can be modeled by different quantum states of the Rydberg atom. These quantum states include the ground state $|1\rangle$, a lowly-excited state $|2\rangle$, and the Rydberg states, which are $|3\rangle$ and $|4\rangle$. The probe beam of angular frequency ω_p excites the quantum state from $|1\rangle \rightarrow |2\rangle$, and the coupling beam of angular frequency ω_c induces the transition $|2\rangle \rightarrow |3\rangle$, transforming the alkali-metal atom to the Rydberg atom. Thereafter, the RF signals of angular frequency ω_{RF} excite the Rydberg state to another Rydberg state $|3\rangle \rightarrow |4\rangle$, enabling the RF signal detection by monitoring the variations induced by these electron transitions via photodetector (PD).

2) *Rabi frequency and detuning*: The interaction strength between the RF signals and the electric dipole moment is characterized by the *Rabi frequency*. The general expression of Rabi frequency Ω_{RF} is given by [7]

$$\Omega_{\text{RF}} = \frac{\mu_{34}}{\hbar} |E_{\text{RF}}|, \quad (4)$$

where μ_{34} , \hbar , and E_{RF} are the transition dipole moment, reduced Planck constant, and RF signals, respectively.

Furthermore, the frequency deviation between the transition frequency and the carrier frequency arises for every electron

transition process due to the discrete energy level, also referred to as *frequency detuning*. For example, the frequency detuning Δ_p presents the gap between ω_p and the transition frequency ω_{12} , i.e., $\Delta_p = \omega_p - \omega_{12}$. Likewise, the detuning of the coupling beam Δ_c and the RF signal Δ_{RF} can be introduced in the same manner so that $\Delta_c = \omega_c - \omega_{23}$ and $\Delta_{\text{RF}} = \omega_{\text{RF}} - \omega_{34}$, where ω_{23} and ω_{34} are transition frequency of coupling beam and RF signals, respectively. The detunings are zero when they are on-resonant with their respective electron transitions. In this work, we assumed the probe beam and the coupling beam are on-resonant with their transitions (i.e., $\Delta_p = \Delta_c = 0$) [13].

3) *Dynamics of quantum state*: The dynamic quantum state is governed by the Lindblad master equation. For the AFDM, we adopt the four-level system model since the deviation of each chirp subcarrier frequency from the transition frequency can be fully described by the different frequency detunings. Based on this system, the Lindblad master equation is represented as [7]

$$\frac{\partial \rho}{\partial t} = -\frac{j}{\hbar} [\mathbf{H}, \rho] + \mathcal{L}, \quad (5)$$

where $[\mathbf{H}, \rho]$ denotes the commutator $\mathbf{H}\rho - \rho\mathbf{H}$. Here, \mathbf{H} , ρ , and \mathcal{L} are the Hamiltonian operator, density matrix, and the decoherence operator, respectively. Here, the Hamiltonian operator \mathbf{H} is given by

$$\mathbf{H} = \frac{\hbar}{2} \begin{bmatrix} 0 & \Omega_p & 0 & 0 \\ \Omega_p & 0 & \Omega_c & 0 \\ 0 & \Omega_c & 0 & \Omega_{\text{RF}} \\ 0 & 0 & \Omega_{\text{RF}} & -2\Delta_{\text{RF}} \end{bmatrix}, \quad (6)$$

where Ω_p , Ω_c , Ω_{RF} , and Δ_{RF} are Rabi frequencies of probe beam, coupling beam, RF signal, and the frequency detunings of RF signal, respectively. The decoherence matrix \mathcal{L} is presented as [7]

$$\mathcal{L} = -\frac{1}{2} \{\mathbf{\Gamma}, \rho\} + \mathbf{\Lambda}, \quad (7)$$

where $\{\mathbf{\Gamma}, \rho\}$ denotes the anti-commutator $\mathbf{\Gamma}\rho + \rho\mathbf{\Gamma}$ and $\mathbf{\Gamma} = \text{diag}\{0, \gamma_2, \gamma_3, \gamma_4\}$. Here, γ_j are the decay rates of the j -th level. The decay matrix is presented as $\mathbf{\Lambda} = \text{diag}\{\gamma_2\rho_{22} + \gamma_4\rho_{44}, \gamma_3\rho_{33}, 0, 0\}$.

4) *Measured optical signal*: The optical measurement, which corresponds to the probe beam output power, can be acquired by solving the steady-state solution of ρ_{12} , which is the (1, 2)-th element of the density matrix ρ . Here, the ρ_{12} is given by [13]

$$\rho_{12} = \frac{A_1 \Omega_{\text{RF}}^2 \Delta_{\text{RF}}^2 + j B_1 \Omega_{\text{RF}}^4}{C_1 \Omega_{\text{RF}}^4 + C_2 \Omega_{\text{RF}}^2 + C_3 \Delta_{\text{RF}}^2}, \quad (8)$$

where $A_1 = 2\Omega_p \Omega_c^2$, $B_1 = \gamma_2 \Omega_p$, $C_1 = 2\Omega_p^2 + \gamma_2^2$, $C_2 = 2\Omega_p^2 (\Omega_c^2 + \Omega_p^2)$, and $C_3 = 4(\Omega_c^2 + \Omega_p^2)^2$.

Let P_{in} represents the input power of the probe beam. Then, according to the adiabatic approximation, the output power of the probe beam P_{out} is defined by the imaginary part of the (1, 2)-th entry of ρ , ρ_{12} , which is presented as [7]

$$P_{\text{out}} = P_{\text{in}} \exp(-C_0 \text{Im}\{\rho_{12}\}), \quad (9)$$

where the constant C_0 is given by $C_0 \triangleq \frac{\Delta^2 N_0 \mu_{12}^2 k_p L}{\epsilon_0 \hbar \Omega_p}$. Here, N_0 , μ_{12} , ϵ_0 , L , and $k_p = \frac{2\pi}{\lambda_p}$ are density of atoms, transition dipole moment of transition $|1\rangle \rightarrow |2\rangle$, vacuum permittivity, length of vapor cell, and wavenumber of probe beam with probe beam wavelength λ_p , respectively.

After the readout of the probe beam power, the PD converts it into the current $I_{\text{out}} = \frac{q\eta}{\hbar\omega_p} P_{\text{out}}$, where η and q are the quantum efficiency of the PD and the charge of electrons. Then, the output voltage is given by [13]

$$V_{\text{out}} = R_T I_{\text{out}} \triangleq V_{\text{in}} \exp(-C_0 \text{Im}\{\rho_{12}\}), \quad (10)$$

where R_T is the load impedance and $V_{\text{in}} \triangleq \frac{R_T q \eta}{\hbar \omega_p} P_{\text{in}}$ is the input voltage.

We define the bias function $\Pi(\Omega, \Delta)$ of the probe beam output power by substituting (8) into (9), as

$$\Pi(\Omega, \Delta) \triangleq V_{\text{in}} \exp\left\{-\frac{B_1 C_0 \Omega^4}{C_1 \Omega^4 + C_2 \Omega^2 + C_3 \Delta^2}\right\}, \quad (11)$$

where $\Omega \in [0, +\infty)$ and $\Delta \in \mathbb{R}$ are the general notation of the Rabi frequency and detuning, respectively.

Furthermore, the gain of the probe beam power $\Upsilon(\Omega, \Delta)$ is derived as a partial derivative of $\Pi(\Omega, \Delta)$, so that $\Upsilon(\Omega, \Delta) \triangleq \frac{\partial \Pi(\Omega, \Delta)}{\partial \Omega}$, where detailed presentation can be found in [13].

III. PROBLEM FORMULATION

A. Measured AFDM Signal Model

Consider a quasi-monostatic sensing of a single moving target in the high-mobility scenario, resulting in a doubly dispersive wireless channel [2]. As illustrated in Fig. 1, we assume the transmitter broadcasts the AFDM signal in downlink to a single moving target and the static Rydberg atomic quantum receiver (RAQR). Following the received AFDM-ISAC signal model in [15], the Rabi frequency of the reference signal Ω_l (line-of-sight only) is

$$\Omega_l = \frac{\mu_{34}}{\hbar} |h_l s(t - \tau') e^{j2\pi\nu_l t}|, \quad (12)$$

where h_l , ν_l , and τ' are the channel gain, Doppler shift, and the propagation delay of the line-of-sight (LOS) path between transmitter and RAQR, respectively. Trivially, $\nu_l = 0$ since the RAQR is fixed without mobility.

We employ the self-heterodyne sensing technique [13], in which the transmitter itself act as the local oscillator (LO) to extract the delay-Doppler from the received signal. In this scheme, the frequency of the measured signal is presented as the phase function between the phase profile difference of LO and the target. Based on (3), the phase function for AFDM $\Delta\phi_m(t, \tau, \tau', \nu_r)$ in a doubly-dispersive channel is given by

$$\begin{aligned} \Delta\phi_m(t, \tau, \tau', \nu_r) &= \phi_m(t - \tau) - \phi_m(t - \tau') + \nu_r t \quad (13) \\ &= (2\tilde{c}_1(\tau' - \tau) + \nu_r) t \\ &\quad + (\tau - \tau') \left(\frac{m}{T} - \frac{q}{\Delta t} + \tilde{c}_1(\tau + \tau') \right), \end{aligned}$$

where $\nu_r = \frac{2v_r \omega_{\text{RF}}}{2\pi c}$ is the Doppler shift of the target, with the relative radial velocity v_r and speed of light c , and the propagation delay of the target-to-RAQR path τ .

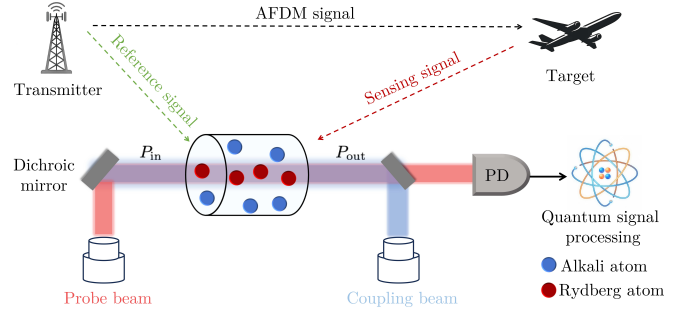


Fig. 1: Quasi-monostatic sensing scenario with AFDM signal for delay-Doppler estimation with RAQRs.

Furthermore, the instantaneous frequency of AFDM coincides with the derivative of $\phi_m(t)$ [14]. Therefore, the frequency detuning of the reference signal at the m -th chirp subcarrier $\Delta_{l,m}(t)$ is presented as

$$\begin{aligned} \Delta_{l,m}(t) &= \frac{d\phi_m(t - \tau')}{dt} - \omega_{34} \quad (14) \\ &= 2\tilde{c}_1 t - 2\tilde{c}_1 \tau' + \frac{m}{T} - \frac{q}{\Delta t} - \omega_{34}. \end{aligned}$$

The noise of the m -th chirp $n_m(t)$ is modeled as Gaussian noise $n_m(t) \sim \mathcal{CN}(0, \sigma_m^2)$, and the intrinsic noise and the extrinsic noise are presented as

$$\begin{aligned} \sigma_{\text{Int},m}^2(t) &= q R_T \Pi(\Omega_l, \Delta_{l,m}(t)), \\ \sigma_{\text{Ext},m}^2(t) &= \frac{\mu_{34}^2}{\hbar^2} \Upsilon^2(\Omega_l, \Delta_{l,m}(t)) \langle E_I^2 \rangle, \quad (15) \end{aligned}$$

where $\langle E_I^2 \rangle = \frac{\hbar \omega_{\text{RF}}^3}{\pi \epsilon_0 c^3} (2n_{\text{th}} + 1)$ is the field intensity of blackbody radiation [13]. Here, ϵ_0 is the dielectric constant and $n_{\text{th}} = 1 / (e^{\hbar \omega_{\text{RF}} / k_B T_E} - 1)$ is the Bose-Einstein distribution, where k_B and T_E are Boltzmann constant and the ambient temperature, respectively.

Given the above, the noise power $\sigma_m^2(t)$ is given by

$$\sigma_m^2(t) = \sigma_{\text{Int},m}^2(t) + \sigma_{\text{Ext},m}^2(t), \quad (16)$$

and consequently, the measured AFDM signal at the m -th chirp subcarrier is presented as

$$\begin{aligned} y_m(t) &= \Pi(\Omega_l, \Delta_{l,m}(t)) + \frac{\mu_{34}}{\hbar} \Upsilon(\Omega_l, \Delta_{l,m}(t)) \\ &\quad \times \frac{1}{N} \sqrt{P_s} \cos(\Delta\phi_m(t, \tau, \tau', \nu_r)) + n_m(t), \quad (17) \end{aligned}$$

where P_s denotes the power of the received signal.

B. Delay-Doppler Parameter Estimation Problem

In light of the measured signal model formulation of AFDM in doubly dispersive channel under RAQRs, the objective of this paper is to accurately estimation the delay-Doppler information of the target $[\tau, \nu_r]$ from the measurements. To achieve this goal, we leverage the atomic autocorrelation property of self-heterodyne sensing, which maps the target's delay to a fluctuation frequency of the output voltage of RAQRs [13].

Mathematically, the instantaneous phase function in (13) is modeled as the fluctuation frequency and the phase of the output voltage, which is presented as

$$\Delta\phi_m(t, \tau, \tau', \nu_r) = -\omega_m t - \varphi_m, \quad (18)$$

where ω_m and φ_m are fluctuation frequency and phase of the $y_m(t)$. Then, by substituting (18) into the (13), the observed fluctuation frequency ω_m is given by

$$\omega_m = 2\tilde{c}_1(\tau - \tau') - \nu_r. \quad (19)$$

From (19), one can observe that the two key parameters to be estimated – time delay τ and the Doppler shift ν_r of the target – are correspondingly embedded in the fluctuation frequency ω_m . In other words, this atomic correlation property of self-heterodyne sensing converts the joint delay-Doppler estimation into the fluctuation frequency estimation problem.

For N subcarriers, we define the frequency vector $\boldsymbol{\omega}$ as

$$\boldsymbol{\omega} = \begin{bmatrix} \omega_0 \\ \vdots \\ \omega_{N-1} \end{bmatrix} = \begin{bmatrix} 2\tilde{c}_1\tau - 2\tilde{c}_1\tau' - \nu_r \\ \vdots \\ 2\tilde{c}_1\tau - 2\tilde{c}_1\tau' - \nu_r \end{bmatrix}, \quad (20)$$

which easily confirms that the estimation problem of τ and ν_r from the fluctuation frequencies $\{\omega_0, \dots, \omega_{N-1}\}$ is an ill-posed linear inverse problem since there are two unknown target parameters, τ and ν_r , with N equivalent equations (i.e., $\omega_0 = \omega_1 = \dots = \omega_{N-1}$). Therefore, with the conventional AFDM, it is highly challenging to extract the delay-Doppler information due to the under-determined system model, which motivates the design of a modified AFDM waveform for the RAQR-enabled joint delay-Doppler estimation.

IV. PROPOSED DUAL-CHIRP AFDM-ENABLED JOINT DELAY-DOPPLER ESTIMATOR

A. Dual-Chirp AFDM

To estimate the delay-Doppler from the optical measurement of RAQRs, we propose a modified AFDM signal, termed as the dual-chirp AFDM, which utilizes two distinct post-chirp rates consecutively, denoted as $c_1^{(A)}$ and $c_1^{(B)}$ respectively. Then, the transmitted signal with a new frame structure of dual-chirp AFDM is described by

$$s(t) = \begin{cases} \sum_{m=0}^{N-1} x[m] e^{j2\pi(c_2 m^2 + \phi_m^{(A)}(t))}, & 0 < t \leq T' \\ \sum_{m=0}^{N-1} x[m] e^{j2\pi(c_2 m^2 + \phi_m^{(B)}(t))}, & T' < t \leq T. \end{cases} \quad (21)$$

where T' is the duration of phase function $\phi_m^{(A)}(t)$ for post-chirp $c_1^{(A)}$. Note that the number of chirp subcarriers for $\phi_m^{(B)}(t)$ is equal to that of $\phi_m^{(A)}(t)$, and the phase function $\phi_m^{(A)}(t)$ and $\phi_m^{(B)}(t)$ of dual-chirp AFDM are given by

$$\begin{aligned} \phi_m^{(A)}(t) &= \tilde{c}_1^{(A)} t^2 + \frac{m}{T'} t - \frac{q}{\Delta t} t, \\ \phi_m^{(B)}(t) &= \tilde{c}_1^{(B)} t^2 + \frac{m}{T - T'} t - \frac{q}{\Delta t} t, \end{aligned} \quad (22)$$

where $\tilde{c}_1^{(A)} = \frac{c_1^{(A)}}{\Delta t^2}$ and $\tilde{c}_1^{(B)} = \frac{c_1^{(B)}}{\Delta t^2}$, respectively.

Then, by substituting (22) into (13), the fluctuation frequency of the m -th subcarrier in (19) is reformulated as

$$\omega_m = \begin{cases} 2\tilde{c}_1^{(A)}(\tau - \tau') - \nu_r, & 0 < t \leq T' \\ 2\tilde{c}_1^{(B)}(\tau - \tau') - \nu_r, & T' < t \leq T. \end{cases} \quad (23)$$

From equation (23), it is trivial that the problem is now solvable since the utilization of the two post-chirps, $c_1^{(A)}$ and $c_1^{(B)}$, introduces an additional distinct equation to the system.

B. Proposed Algorithm

1) *Fluctuation frequency estimation*: We first estimate the fluctuation frequency of the measured signal. Here, we adopt the nonlinear least square (NLS)-based optimization algorithm in [13]. First, the normalized received signal of the m -th chirp subcarrier is presented as

$$\begin{aligned} \bar{y}_m(t) &= \frac{y_m(t) - \Pi(\Omega_l(t), \Delta_{l,m}(t))}{\sigma_m(t)} \\ &= \varrho_m(t) h \cos(\omega_m t + \varphi_m) + \bar{n}_m(t), \end{aligned} \quad (24)$$

where $\bar{n}_m(t)$ is a unit power of Gaussian noise and h denotes a gain of LOS channel. Here, the amplitude $\varrho_m(t)$ is given by

$$\varrho_m(t) = \frac{\mu_{34} \Upsilon(\Omega_l, \Delta_{l,m}(t)) \sqrt{P_s}}{\hbar \sqrt{N(\sigma_{\text{Int},m}^2(t) + \sigma_{\text{Ext},m}^2(t))}}. \quad (25)$$

To ease the expression, consider a time duration for $\phi_m^{(A)}(t)$. Then, following the NLS problem in [13], the frequency estimation problem is presented as

$$\max_{\boldsymbol{\omega}_m^{(0)}} \left| \int_0^{T'} \bar{y}_m(t) \varrho_m(t) e^{j\omega_m^{(0)} t} dt \right|^2. \quad (26)$$

The peaks of $\left| \int_0^{T'} \bar{y}_m(t) \varrho_m(t) e^{j\omega_m^{(0)} t} dt \right|^2$ can be observed via time-frequency analysis technique such as fast Fourier transform (FFT), where its location $\boldsymbol{\omega}^{(0)} = [\omega_0^{(0)}, \dots, \omega_{N-1}^{(0)}]^T$ represents the estimated frequency for all chirp subcarriers.

After the initial estimation, the refinement is conducted to enhance the accuracy. By using Newton's method, the refinement is presented as

$$\begin{pmatrix} \hat{\omega}_m^{(t)} \\ \hat{\varphi}_m^{(t)} \end{pmatrix} = \begin{pmatrix} \hat{\omega}_m^{(t-1)} \\ \hat{\varphi}_m^{(t-1)} \end{pmatrix} + \begin{pmatrix} \frac{\partial^2 Q}{\partial \hat{\omega}_m^2} & \frac{\partial^2 Q}{\partial \hat{\omega}_m \partial \hat{\varphi}_m} \\ \frac{\partial^2 Q}{\partial \hat{\varphi}_m \partial \hat{\omega}_m} & \frac{\partial^2 Q}{\partial \hat{\varphi}_m^2} \end{pmatrix}^{-1} \begin{pmatrix} \frac{\partial Q}{\partial \hat{\omega}_m} \\ \frac{\partial Q}{\partial \hat{\varphi}_m} \end{pmatrix}, \quad (27)$$

for $m = 0, 1, \dots, N - 1$. Here, $Q \triangleq Q(\hat{\omega}_m, \hat{\varphi}_m)$ is an objective function, which is presented as

$$Q(\hat{\omega}_m, \hat{\varphi}_m) \triangleq \frac{\left| \int_0^{T'} \bar{y}(t) \varrho(t) \cos(\hat{\omega}_m t + \hat{\varphi}_m) dt \right|^2}{\int_0^{T'} |\varrho(t) \cos(\hat{\omega}_m t + \hat{\varphi}_m)|^2 dt}. \quad (28)$$

Once the updated $Q(\hat{\omega}_m^{(t)}, \hat{\varphi}_m^{(t)})$ is larger than the previous one, the iteration is completed and the final estimated frequency is given by $\hat{\omega}_m^{(T_{\text{iter}})}$, where T_{iter} is the number of total iterations for $m = 0, 1, \dots, N - 1$.

Eventually, the final estimated frequency can be acquired by taking the average of the estimated frequency, which are presented as $\hat{\omega}^{(A)} = \frac{1}{N} \sum_{m=0}^{N-1} \hat{\omega}_m^{(T_{\text{iter}})}$. Likewise, the final estimated frequency for frame B , $\hat{\omega}^{(B)} = \frac{1}{N} \sum_{m=0}^{N-1} \hat{\omega}_m^{(T_{\text{iter}})}$, can be acquired in a same manner by following (26)-(28) for duration $T' < t \leq T$.

2) *LS-based Delay-Doppler Estimation*: With the estimated fluctuation frequency $\hat{\omega}^{(A)}$ and $\hat{\omega}^{(B)}$, the problem can be formulated based on the LS criterion. Specifically, the fluctuation frequency can be presented as

$$\underbrace{\begin{bmatrix} \hat{\omega}^{(A)} \\ \hat{\omega}^{(B)} \end{bmatrix}}_{\hat{\omega} \in \mathbb{R}^{2 \times 1}} = \underbrace{\begin{bmatrix} 2\tilde{c}_1^{(A)} & -1 \\ 2\tilde{c}_1^{(B)} & -1 \end{bmatrix}}_{\triangleq \mathbf{C}_1 \in \mathbb{R}^{2 \times 2}} \underbrace{\begin{bmatrix} \tau - \tau' \\ \nu_r \end{bmatrix}}_{\vartheta}, \quad (29)$$

where $\hat{\omega}$ is the estimated frequency vector, \mathbf{C}_1 is the post-chirp matrix for dual-chirp AFDM, and ϑ is the parameter set of delay-Doppler. Note that \mathbf{C}_1 is a full-rank only if $\tilde{c}_1^{(A)} \neq \tilde{c}_1^{(B)}$, which is accomplished by the proposed dual-chirp AFDM, and not for the conventional AFDM¹.

Finally, applying the LS method on (29), we obtain the vector ϑ as

$$\vartheta = (\mathbf{C}_1^\top \mathbf{C}_1)^{-1} \mathbf{C}_1^\top \hat{\omega}, \quad (30)$$

which yields the estimated delay and Doppler as $\hat{\tau} = [\vartheta]_1 + \tau'$ and $\hat{\nu}_r = [\vartheta]_2$, where $[\vartheta]_1$ and $[\vartheta]_2$ are the first and the second elements of ϑ , respectively.

V. SIMULATION RESULTS

A. Simulation Environment

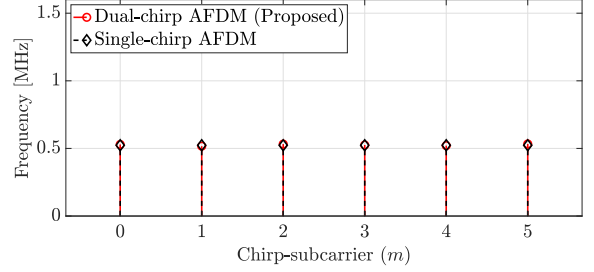
Unless stated otherwise, the default setting of the simulations is organized in Table. I. The average received signal-to-noise ratio (SNR) considering the time-varying amplitude $q_m(t)$, is defined as

$$\text{SNR}(t) \triangleq \frac{1}{N} \sum_{m=0}^{N-1} q_m^2(t) h^2 T. \quad (31)$$

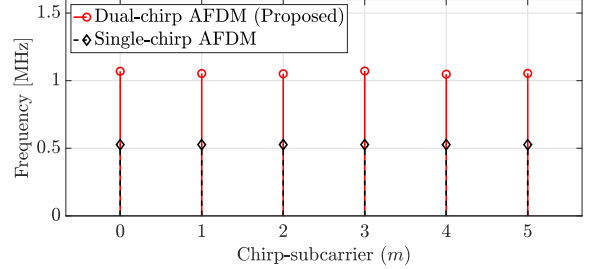
TABLE I: Parameters for simulations

Description	Parameter	Value
Energy levels	{ 1⟩, 2⟩}	{6S _{1/2} , 6P _{3/2} }
Energy levels	{ 3⟩, 4⟩}	{60D _{5/2} , 63P _{3/2} }
Frequency	ω_{RF}	$2\pi \times 62.76$ GHz
Number of chirp-subcarriers	N	6
Transition dipole moments	{ μ_{12}, μ_{34} }	{2.586, 229} qa_0
Bohr radius	a_0	52.9 pm
Length of vapor cell	L	0.02 m
Rabi frequencies	{ Ω_p, Ω_c }	$2\pi \times \{5.8, 1\}$ MHz
Wavelengths	{ λ_p, λ_c }	{852, 509} nm
Decay rate	γ_2	$2\pi \times 5.2$ MHz
Quantum efficiency	η	0.8
Target range	L	1,000 m
Transmitter-to-RARQ distance	L'	1 m
Velocity	ν_r	50 m/s
Bandwidth	B	1 MHz
Pre-chirp parameter	c_2	$\sqrt{2}$
Density of atoms	N_0	$4.89 \times 10^{16} \text{ m}^{-3}$

¹Notice that the number of unique chirp rates may be artificially increased (i.e., $c_1^{(C)}, c_1^{(D)}, \dots$) to obtain an over-determined system to further improve the accuracy of the proposed algorithm, but this trivial extension is not investigated in this article.



(a) FFT spectrum of duration $0 < t \leq T'$.



(b) FFT spectrum of duration $T' < t \leq T$.

Fig. 2: FFT spectrum comparison between single-chirp AFDM and the proposed dual-chirp AFDM, highlighting the different spectra between the two frames of the dual-chirp AFDM, compared to the identical spectra of the conventional AFDM.

Note that the received SNR remains constant when the transmission power is fixed [13]. For the estimation performance analysis, we adopted the normalized normalized root mean square error (NRMSE), which is defined as [5]

$$\text{NRMSE} = \mathbb{E} \left[\frac{1}{|\zeta|} \sqrt{(\hat{\zeta} - \zeta)^2} \right], \quad (32)$$

where $\mathbb{E}[\cdot]$ is the expectation and ζ denotes a given channel parameter (range or velocity) and $\hat{\zeta}$ is its estimate.

B. Performance Analysis

In this subsection, we analyze the estimation performance of the proposed dual-chirp AFDM. For the comparison of the delay-Doppler estimation performance, the classical single-chirp AFDM is adopted. To establish a practical performance baseline, the post-chirp difference $\Delta c_1 = c_1^{(B)} - c_1^{(A)}$ is introduced to approximate the behavior of conventional single-chirp AFDM. This formulation is necessary because having exactly identical chirp rates ($c_1^{(A)} = c_1^{(B)}$), and $\Delta c_1 = 0$ results in a rank-1 measurement matrix \mathbf{C}_1 , which limits the use of LS-based delay-Doppler estimation. By utilizing this approximation, the performance of the conventional framework can be effectively modeled for comparative purposes, while in truth, unambiguous joint delay-Doppler estimation with conventional AFDM is not possible. In the simulation for the single-chirp AFDM, we set Δc_1 as 10^{-3} .

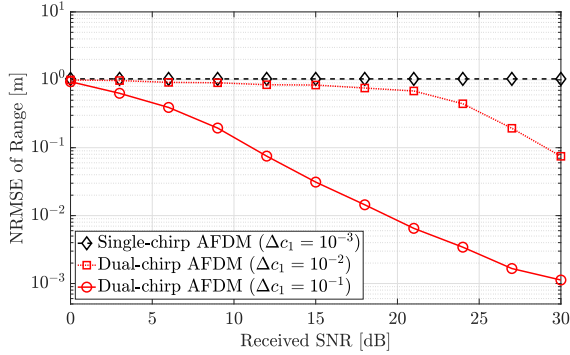
First, Fig. 2 presents the results of the FFT spectrum analysis, where the average received SNR is fixed at 30 dB.

VI. CONCLUSION

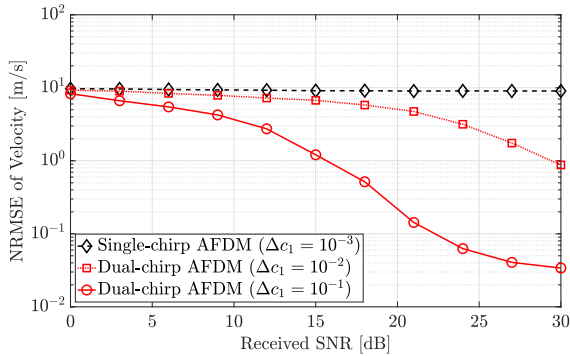
In this paper, we proposed the dual-chirp AFDM, the first waveform tailored for RAQR-based joint delay-Doppler estimation. By employing distinct post-chirp rates, the proposed framework ensures a full-rank measurement matrix for the delay and Doppler parameters, facilitating accurate parameter recovery via NLS and LS algorithms. Numerical results validate the superior performance of dual-chirp AFDM, establishing it as a robust solution for emerging quantum sensing and ISAC applications.

REFERENCES

- [1] F. Liu, Y. Cui, C. Masouros, J. Xu, T. X. Han, Y. C. Eldar, and S. Buzzi, "Integrated sensing and communications: Toward dual-functional wireless networks for 6G and beyond," *IEEE J. Sel. Areas Commun.*, vol. 40, no. 6, pp. 1728–1767, Jun. 2022.
- [2] H. S. Rou et al., "From orthogonal time–frequency space to affine frequency-division multiplexing: A comparative study of next-generation waveforms for integrated sensing and communications in doubly dispersive channels," *IEEE Sig. Process. Mag.*, vol. 41, no. 5, pp. 71–86, Sep. 2024.
- [3] A. Bemani, N. Ksairi, and M. Kountouris, "Affine frequency division multiplexing for next generation wireless communications," *IEEE Trans. Wireless Commun.*, vol. 22, no. 11, pp. 8214–8229, Nov. 2023.
- [4] H. S. Rou, K. R. R. Ranasinghe, V. Savaux, G. T. F. de Abreu, D. González G., and C. Masouros, "Affine Frequency Division Multiplexing (AFDM) for 6G: Properties, Features, and Challenges," *IEEE Commun. Stand. Mag.*, pp. 1–10, 2026.
- [5] K. R. R. Ranasinghe, H. S. Rou, G. T. F. de Abreu, T. Takahashi, and K. Ito, "Joint channel, data, and radar parameter estimation for AFDM systems in doubly-dispersive channels," *IEEE Trans. Wireless Commun.*, vol. 24, no. 2, pp. 1602–1619, Feb. 2025.
- [6] T. Gong et al., "Rydberg atomic quantum receivers for classical wireless communication and sensing," *IEEE Wireless Communications*, vol. 32, no. 5, pp. 90–100, Oct. 2025.
- [7] M. Jing, Y. Hu, J. Ma, H. Zhang, L. Zhang, L. Xiao, and S. Jia, "Atomic superheterodyne receiver based on microwave-dressed Rydberg spectroscopy," *Nat. Phys.*, vol. 16, no. 9, pp. 911–915, Jun. 2020.
- [8] H. Kim, H. Park, and S. Kim, "Quantum-MUSIC: Multiple signal classification for quantum wireless sensing," *IEEE Wireless Commun. Lett.*, vol. 14, no. 6, pp. 1623–1627, Jun. 2025.
- [9] M. Guo, Y. Guo, X. Guo, C. Guo, and Y. Wang, "Ultra-high precision LEO Doppler localization facilitated by Rydberg atomic receivers," *IEEE Trans. Veh. Tech.*, 2025.
- [10] M. Chen, T. Mao, Y. Zhao, W. Xiao, D. Zheng, Z. Wang, J. Zhang, and S. Chen, "New paradigm for integrated sensing and communication with Rydberg atomic receiver," *IEEE Commun. Mag.*, vol. 63, no. 12, pp. 104–111, Dec. 2025.
- [11] M. Cui, Q. Zeng, and K. Huang, "Towards atomic MIMO receivers," *IEEE J. Sel. Areas Commun.*, vol. 43, no. 3, pp. 659–673, Mar. 2025.
- [12] T. Gong, J. Sun, C. Yuen, G. Hu, Y. Zhao, Y. L. Guan, C. M. S. See, M. Debbah, and L. Hanzo, "Rydberg atomic quantum receivers for classical wireless communications and sensing: Their models and performance," *arXiv preprint arXiv:2412.05554*, 2024.
- [13] M. Cui, Q. Zeng, Z. Wang, and K. Huang, "Realizing quantum wireless sensing without extra reference sources: Architecture, algorithm, and sensitivity maximization," *arXiv preprint arXiv:2504.21234*, 2025.
- [14] A. Bemani, N. Ksairi, and M. Kountouris, "Integrated sensing and communications with affine frequency division multiplexing," *IEEE Wireless Commun. Lett.*, vol. 13, no. 5, pp. 1255–1259, Feb. 2024.
- [15] H. Yin et al., "Ambiguity function analysis of AFDM signals for integrated sensing and communications," *IEEE J. Sel. Areas Commun.*, vol. 44, pp. 196–211, Feb. 2026.
- [16] Y. I. Tek and E. Basar, "A novel and secure AFDM system for high mobility environments," *IEEE Trans. Veh. Tech.*, vol. 74, no. 12, pp. 19 945–19 950, Dec. 2025.



(a) NRMSE of range.



(b) NRMSE of velocity.

Fig. 3: Joint range-velocity NRMSE performance versus SNR.

The post-chirp rates for the dual-chirp AFDM are set to $c_1^{(A)} = \frac{3}{2N}$ and $c_1^{(B)} = \frac{6}{2N}$, while the single-chirp baseline utilizes $c_1^{(A)} = \frac{3}{2N}$ and $c_1^{(B)} = c_1^{(A)} + \Delta c_1$.

As illustrated in the figures, the proposed dual-chirp AFDM results in two distinct spectral peaks across the periods $0 < t \leq T'$ (Fig. 2a) and $T' < t \leq T$ (Fig. 2b). In contrast, the conventional AFDM exhibits nearly identical peaks across both frames, failing to provide additional information for parameter decoupling. This confirms that the dual-chirp structure effectively generates unique frequency measurements, thereby eliminating the inherent ambiguity in the RAQR readout.

Next, Fig. 3 illustrates the NRMSE performance for range and velocity estimation using the proposed approach. As expected, the single-chirp AFDM baseline (approximated via marginal Δc_1) exhibits poor estimation accuracy across the entire SNR range. This error floor stems from the inherent structural ambiguity of the single-chirp waveform, where nearly identical frequency measurements across all subcarriers prevent the decoupling of delay and Doppler parameters.

In contrast, the proposed dual-chirp AFDM achieves significantly superior performance. Furthermore, it is observed that increasing the post-chirp difference Δc_1 leads to an enhancement in estimation accuracy. This behavior is attributed to the conditioning of the post-chirp matrix \mathbf{C}_1 , where a negligible Δc_1 makes the matrix near-singular and ill-conditioned, while a sufficient difference restores the full-rank status of \mathbf{C}_1 , thereby enabling robust and unambiguous joint estimation.